AD-A040 286 CALSPAN CORP BUFFALO N Y F/G 20/4
REYNOLDS NUMBER EFFECTS ON THE SHOCK WAVE-TURBULENT BOUNDARY LA--ETC(U)
JUL 73 R J VIDAL, C E WITTLIFF, P A CATLIN F44620-71-C-0046
UNCLASSIFIED AFOSR-TR-77-0686 NL

1 OF 1
AD
A040286

END

DATE
FILMED
6-77

UNCLASSIFIED

SECURITY CLASSIFICATION OF THIS PAGE (When Data Entered)

REPORT DOCUMENTATION PAGE

READ INSTRUCTIONS BEFORE COMPLETING FORM

1. REPORT NUMBER (18) AFOSR - TR-77-0686 (19)
2. GOVT ACCESSION NO. (2)
3. RECIPIENT'S CATALOG NUMBER

4. TITLE (and Subtitle)
REYNOLDS NUMBER EFFECTS ON THE SHOCK WAVE-TURBULENT BOUNDARY LAYER INTERACTION AT TRANSONIC SPEEDS.

5. TYPE OF REPORT & PERIOD COVERED
INTERIM (9) Rept. for 15 Jan 73 — 15 Jan 74,
6. PERFORMING ORG. REPORT NUMBER

7. AUTHOR(s) (10)
R. J. VIDAL, B. H. SHEEN
C. E. WITTLIFF,
P. A. CATLIN

8. CONTRACT OR GRANT NUMBER(s)
(15) F44620-71-C-0046,
N0014-71-C-0165

9. PERFORMING ORGANIZATION NAME AND ADDRESS
CALSPAN CORPORATION
PO BOX 235
BUFFALO, NEW YORK 14221

10. PROGRAM ELEMENT, PROJECT, TASK AREA & WORK UNIT NUMBERS
(16) 9781-01
61102F (17)

11. CONTROLLING OFFICE NAME AND ADDRESS
AIR FORCE OFFICE OF SCIENTIFIC RESEARCH/NA (11)
1400 WILSON BOULEVARD
ARLINGTON, VIRGINIA 22209

12. REPORT DATE
Jul 73
13. NUMBER OF PAGES
14 (12) 17p.

14. MONITORING AGENCY NAME & ADDRESS (if different from Controlling Office)

15. SECURITY CLASS. (of this report)
UNCLASSIFIED
15a. DECLASSIFICATION/DOWNGRADING SCHEDULE

16. DISTRIBUTION STATEMENT (of this Report)

Approved for public release; distribution unlimited.

17. DISTRIBUTION STATEMENT (of the abstract entered in Block 20, if different from Report)

18. SUPPLEMENTARY NOTES
PROCEEDINGS
AIAA FLUID AND PLASMA DYNAMICS CONFERENCE 6th Palm Springs, California
pp1-14 16-18 July 1973

19. KEY WORDS (Continue on reverse side if necessary and identify by block number)
TRANSONICS
SHOCK WAVE-BOUNDARY LAYER INTERACTION
TWO DIMENSIONAL
SEPARATED FLOW

20. ABSTRACT (Continue on reverse side if necessary and identify by block number)
A Ludwieg tube experiment is described in which the pertinent features of the shock wave-boundary layer interaction on an airfoil are simulated with a two-dimensional flat plate in a supersonic nozzle. The nozzle is modified to impress an airfoil pressure distribution on the flat plate that is typical of a cruising flight condition. A normal shock wave is positioned at a fixed location on the plate, and measurements are made in the vicinity of the shock wave-boundary layer interaction zone. The measurements made are Fastex schlieren motion pictures of the flowfield, pitot and static pressure surveys normal to the surface, and skin

DD FORM 1 JAN 73 1473 EDITION OF 1 NOV 65 IS OBSOLETE

UNCLASSIFIED 407727

SECURITY CLASSIFICATION OF THIS PAGE (When Data Entered)

friction and surface pressure distributions in the interaction zone. The test conditions nominally are a Mach number of 1.4 ahead of the shock wave and a Reynolds number, based on shock position, of 9 million or 36 million. The Schilieren observations show that the shock wave-boundary layer interaction is steady only in a mean sense since the geometry of the bifurcated shock wave at the surface changes with time. The surface measurements show that at the lowest Reynolds number, there is a region of separated flow downstream of the shock wave that extends about nine (undisturbed) boundary layer thicknesses. This separated region decreases to about one or two (undisturbed) boundary layer thicknesses at the higher Reynolds number. This finding is confirmed by the measured velocity profiles which show that the disturbed viscous layer tends to recover normal boundary layer characteristics more rapidly at the higher Reynolds number.

AIAA Paper
No. 73-661

REYNOLDS NUMBER EFFECTS ON THE SHOCK WAVE -- TURBULENT BOUNDARY LAYER INTERACTION AT TRANSONIC SPEEDS

by
R. J. VIDAL, C. E. WITTLIFF, P. A. CATLIN,
and
B. H. SHEEN
Calspan Corporation
Buffalo, New York

AIAA 6th Fluid and Plasma Dynamics Conference

PALM SPRINGS, CALIFORNIA / JULY 16-18, 1973

REYNOLDS NUMBER EFFECTS ON THE SHOCK WAVE - TURBULENT BOUNDARY LAYER INTERACTION AT TRANSONIC SPEEDS*

R.J. Vidal,** C.E. Wittliff,** P.A. Catlin,† and B.H. Sheen‡
Aerodynamic Research Department
Calspan Corporation,
Buffalo, N.Y.

Abstract

A Ludwieg tube experiment is described in which the pertinent features of the shock wave-boundary layer interaction on an airfoil are simulated with a two-dimensional flat plate in a supersonic nozzle. The nozzle is modified to impress an airfoil pressure distribution on the flat plate that is typical of a cruising flight condition. A normal shock wave is positioned at a fixed location on the plate, and measurements are made in the vicinity of the shock wave-boundary layer interaction zone. The measurements made are Fastex schlieren motion pictures of the flowfield, pitot and static pressure surveys normal to the surface, and skin friction and surface pressure distributions in the interaction zone. The test conditions nominally are a Mach number of 1.4 ahead of the shock wave and a Reynolds number, based on shock position, of 9 million or 36 million. The schlieren observations show that the shock wave-boundary layer interaction is steady only in a mean sense since the geometry of the bifurcated shock wave at the surface changes with time. The surface measurements show that at the lowest Reynolds number, there is a region of separated flow downstream of the shock wave that extends about nine (undisturbed) boundary layer thicknesses. This separated region decreases to about one or two (undisturbed) boundary layer thicknesses at the higher Reynolds number. This finding is confirmed by the measured velocity profiles which show that the disturbed viscous layer tends to recover normal boundary layer characteristics more rapidly at the higher Reynolds number.

Nomenclature

c	airfoil chord length
C_f	skin friction coefficient, $\tau/\frac{1}{2}\rho_\infty u_\infty^2$
C_p	pressure coefficient, $(p-p_\infty)/\frac{1}{2}\rho_\infty u_\infty^2$
D	nozzle diameter
F_c, F_{Rx}	coefficients from Spaulding and Chi, Ref. 13
M	Mach number
n	exponent for a power-law profile, $u/u_e = (y/\delta)^{1/n}$
p	pressure
Re	Reynolds number
T	temperature
u	chordwise velocity
x	chordwise coordinate, measured from leading edge
y	coordinate normal to the surface
β	empirical constant from Stratford, Ref. 12
γ	ratio of specific heads
δ	boundary layer thickness
δ^*	boundary layer displacement thickness
θ	boundary layer momentum thickness
ρ	density
σ	porosity, ratio of open to total area
τ	skin friction

Subscripts

e	boundary layer edge conditions
i	initial conditions
o	reservoir conditions
s	shock wave location
u	undisturbed condition
w	wall condition
∞	ambient conditions

Introduction

A program of research is in progress at the Calspan Corporation to investigate experimentally the interaction between a shock wave and a turbulent boundary layer typical of that occurring on an aircraft wing at transonic speeds. The need for this research is illustrated by the results given by Loving[1]. He reports on flight test experiments with the C141 airplane and compares those high Reynolds number results with lower Reynolds number wind tunnel results. He found that the center of pressure at transonic speeds was as much as 15% of the wing chord aft of the position determined in wind tunnel experiments. Comparisons between wing pressure distributions showed that this difference stemmed from a rearward shift of the supercritical shock wave in the flight tests, and demonstrated the need for developing criteria for scaling shock wave-boundary layer interactions. There are no basic data to use in establishing criteria on such interactions at full-scale Reynolds numbers. The present research is intended to provide those basic data and thereby to establish a basis for developing scaling criteria.

The present research centers on a simulation experiment conducted in the Calspan Ludwieg tube. The basic principles of a Ludwieg tube are described in the literature[2-4], and if one neglects the starting process, it can be regarded as a short duration blowdown wind tunnel. The present simulation experiment uses a cylindrical, perforated wall nozzle which is contained within an evacuated dump tank. During an experiment, there is flow through the porous walls which produces a supersonic expansion within the nozzle. By selectively covering the wall perforations, it is possible to control the expansion and duplicate the supersonic portions of the chordwise pressure distribution on an airfoil. The airfoil boundary layer is developed on a flat plate that spans the nozzle, and the shock wave-boundary layer interaction is produced by choking the flow at the exit of the apparatus and positioning the shock wave on a suitable shock holder.

The details of the experimental apparatus and instrumentation are described in the next section, and this is followed by a description of the methods used in reducing the data. Following that, the experimental results are presented and discussed.

*Sponsored by ONR, Contract No. N00014-71-C-0165 and AFOSR, Contract No. F44620-71C-0046.
**Principal Engineer
†Junior Engineer
‡Associate Engineer

Experimental Apparatus

As indicated in the Introduction, the present experiments were made in the Calspan Ludwieg tube. This facility is described in detail in Ref. 4 and is illustrated in Fig. 1. It consists of a 30 ft. long supply tube with an inner diameter of 42 inches. It has a diaphragm station between the supply tube and the nozzle, and the latter exhausts into a dump tank 8 ft. in diameter and 30 ft. long. In performing an experiment, plastic diaphragms are inserted at the diaphragm station, the nozzle and dump tank are evacuated to a predetermined pressure, the supply tube is pressurized, and the diaphragms are ruptured mechanically. After the transient starting process is completed, a steady flow is obtained for the length of time required for the expansion wave to travel up the supply tube, reflect from the end wall, and propagate downstream to the nozzle; nominally 45 to 50 milliseconds for this tube configuration.* The facility is designed to operate at Reynolds numbers up to 40 million per foot.

The sketch in Fig. 1 shows the facility with a Mach number 2 nozzle installed. Three other nozzles are available; solid wall nozzles for M=3.5 and 4.5, and a perforated wall nozzle 32 inches in diameter for transonic testing. The latter was used in the present research with the supply tube translated forward so that the perforated portion of the nozzle was contained within the evacuated dump tank.

The Simulation Experiment

The basic aim in the present research is to impress an airfoil pressure distribution on a flat plate that spans the nozzle, and to study the interaction between a normal shock wave and the turbulent boundary layer that develops on the flate plate. Since the perforated nozzle is contained within the evacuated dump tank, there is an outflow through the porous walls during the experiment that produces a supersonic expansion. It is possible to control this expansion by selectively covering the wall perforations and thereby obtain a specified axial pressure distribution in the nozzle. The method used here to select a distribution of wall porosity follows that given by Sheeran and Hendershot[4] with certain modifications. The method is based on the observation that since the nozzle is exhausting into an evacuated dump tank, the flow through the perforated walls is choked. This makes it possible to write down a mass balance for the flow as a function of distance from the throat, and in that way obtain a solution for the required porosity distribution as a function of the desired Mach number distribution. Neglecting the details of this development, it can be shown that mass conservation requires that

$$\left(\frac{\gamma+1}{2}\right)^{\frac{\gamma+1}{2(\gamma-1)}} \frac{M(x)}{\left[1+\frac{\gamma+1}{2}M^2(x)\right]^{\frac{\gamma+1}{2(\gamma-1)}}} = 1-\int_0^x \frac{40^\circ C\, d(x/D)}{\left[1+\frac{\gamma+1}{2}M^2(x)\right]^{\frac{\gamma+1}{2(\gamma-1)}}} \quad (1)$$

*Modifications are now in progress to double the length of the supply tube and hence double the test time.

and it follows that the axial distribution of porosity is given by

$$40^\circ C = \left(\frac{\gamma+1}{2}\right)^{\frac{\gamma+1}{2(\gamma-1)}} \left[\frac{M^2(x)-1}{1+\frac{\gamma-1}{2}M^2(x)}\right] \frac{dM(x)}{d(x/D)} \quad (2)$$

Equation 2 was used in combination with flight test pressure data to design the porosity distribution for the present experiment.

The nozzle-flat plate arrangement is shown schematically in Fig. 2. The leading edge of the flat plate is located about half an inch ahead of the nozzle throat and extends beyond the nozzle exit. The flow downstream of the nozzle exit is constrained by a rectangular observation section starting at the nozzle exit. The flow is choked with an adjustable flap at the exit of the rectangular observation section, and this produces a normal shock wave which propagates upstream with a strength, M ≈ 1.65.

One important aspect of the experimental design was the selection of a shock holder which would stop the traveling shock wave and stabilize it at a fixed position. This problem can be regarded as a non-steady shock tube problem and was analyzed using existing theories for shock tubes[5,6]. These show that a propagating shock wave can be weakened and positioned at a fixed location by introducing an area change. The shock holder shown in Fig. 2 was designed using relations from Ref. 6 to decrease the strength of the propagating shock wave so that it would be stable in the M = 1.4 flow.

Model and Instrumentation

The model forms an integral part of the Ludwieg tube and consists of a flat plate approximately twelve feet long with a rectangular observation section at the downstream end. It is constructed from solid aluminum plate 1-1/4 inches thick, and the assembled unit is shown in Fig. 3 and 4. Figure 3 is a view from the nozzle entrance and shows the leading edge of the flat plate slightly ahead of the nozzle throat. There are a total of seventeen Mylar cover plates distributed around the nozzle circumference to define the porosity distribution necessary to produce the desired airfoil pressure distribution. The rectangular observation section with the choking flap can be seen at the downstream end.

A view from the downstream end of the apparatus is shown in Fig. 4. This shows the apparatus as originally conceived with a solid cover plate over the aft 40% of the nozzle. The early experiments showed there were compression waves entering the observation section, and the solid cover plate was replaced with an extension of the Mylar cover plates Fig. 3, to provide a continuation of the upstream porosity distribution. Figure 4 shows that the observation section is a rectangular box extending about three inches into the nozzle and serves to define a flow field without the thick nozzle boundary layer. The choking flap is normal to the flow and the height can be adjusted to position the normal shock wave in the observation section. A series of experiments was made with and without a smooth fairing upstream of the flap. There was no discernible difference in the flow quality or the starting

time, and all subsequent experiments have been made without the fairing.

All model instrumentation is contained within the model. There are ten separate instrumentation ports upstream of the observation section to verify the desired surface pressure distribution and to measure local skin friction. There is also a slot milled along the plate centerline in the observation section to accept transducer assemblies and rake assemblies. These units can be positioned axially at one inch intervals to survey the interaction zone.

The instrumentation and the aerodynamic surfaces of the skin friction and surface pressure survey plate are shown in Fig. 5 and 6. These transducers are piezoelectric devices designed and built at the Calspan Corporation and are described in Ref. 7 and 8. Each is compensated internally to minimize acceleration effects and typically they are linear to within ±2%. The pressure transducers can be used up to about 100 psi and have a nominal sensitivity of about 50 mv/psi. The skin friction transducers have 1/4 inch diaphragms and can be used to measure skin friction as large as 0.02 psi. Typically they have skin friction sensitivity of about 25000 mv/psi and a pressure sensitivity 5 to 20 mv/psi. All skin friction transducers were calibrated for pressure sensitivity and corrections were applied to the skin friction data. This was accomplished using the pressure measured adjacent to each skin friction transducer, Fig. 6. It will be noted in Fig. 6 that the skin friction transducers are mounted with the diaphragms flush with the surface and with a 0.010 inch gap around the periphery. Previous checks were made with the gap filled with silicon oil and it was concluded that the gap did not affect the measurements.

Surveys of the viscous flowfield were made using assemblies of a transducer plate and rake plates, Fig. 7. Twenty pressure transducers are mounted on the undersurface of the transducer plate and are vented to the upper surface through conical holes. The hypodermic tubes from the rake plate are fitted with "O" rings that plug into the conical holes to provide a pressure seal when the plates are clamped together. These assemblies were pressure checked and found to have a leak rate of less than 1% per hour.

Typical rake assemblies are shown in Fig. 8 and 9. The assembly shown in Fig. 8 was designed to survey the flowfield 1/3 inch above the surface, and each array is made up of five hypodermic tubes with an o.d. of 0.032 inches. The static rakes are terminated at the front edge by a wedge and have 0.020 inch holes drilled through each side. The second rake, Fig. 9, is typical of the rakes used to survey the outer flowfield when it was supersonic. It consists of two arrays, one having 10 pitot tubes and one having 5 static tubes. These taller rakes were restricted to two arrays in order to insure that the channel between the arrays would not choke. Alternate pitot tubes are bent laterally and buried within the plate to mate with the transducer plate. The static pressure array was limited to five tubes to minimize interference between adjacent tubes. The orifices are 0.008 inch holes located at ±30° from the bottom centerline of the tube to minimize the effects of upflow on the measurements. A third rake, similar to that in Fig. 9 was used to survey the flowfield to 4-3/4" above the plate. Another set of rakes with four arrays of pitot-static tubes, similar to Fig. 8, was used to survey the subsonic flowfields.

The data taken to determine the ambient flow conditions were the total pressure ahead of the nozzle, and the supply tube pressure and temperature immediately before an experiment. In addition schlieren observations of the flowfield were made using a Fastex framing camera operating at a rate of about 7000 frames per second. This diagnostic was also used to determine the time interval when the shock wave is stabilized on the stockholder.

Operational Mode

The usual mode of operation for the Calspan Ludwieg tube is with a very high diaphragm pressure ratio; that is, the dump tank is evacuated to a near-vacuum. A detailed wave diagram analysis was made in designing the experiment to determine if the 50 millisecond test time was sufficient to start the nozzle, establish a stable normal shock wave, and establish a steady viscous interaction.* This study showed that the test time might not be sufficient and it was concluded that the starting time would be minimized if the facility were operated at a diaphragm pressure ratio that would immediately establish sonic flow at the nozzle throat. It was necessary to determine this diaphragm pressure ratio experimentally, and it was found that a value of about twenty was optimum. The total flow time is about fifty milliseconds, and with this mode of operation, a steady inviscid flow is established in about five milliseconds. A steady boundary layer flow, as evidenced by pitot pressure, static pressure, and skin friction, is established about fifteen milliseconds after the start of the experiment. This is consistent with the time required to establish turbulent boundary layers as measured by Davies and Bernstein[9]. An additional ten milliseconds is required for the normal shock wave to propagate upstream from the choking flap to the shock holder, leaving about twenty-five milliseconds for data acquisition. It has been found experimentally that a steady separated flow is established about four to five milliseconds after the shock wave is stabilized, and typically data are taken over a ten millisecond interval.

Data Reduction

The test conditions in the Ludwieg tube were determined by measuring the temperature and pressure in the supply tube immediately before the diaphragm was ruptured, and by measuring the total pressure ahead of the nozzle throat during the experiment. These were used with the isentropic relations and the relation for a centered expansion wave to determine the ambient gas properties.

The pitot pressure and static pressure data obtained in the flow field surveys were reduced to Mach number profiles using the isentropic relations and taking account of the normal shock losses in pitot pressure. It was assumed that the measured static pressure was the true local static pressure. This was verified by comparing these with the wall pressure measured without the rake

*The authors acknowledge the assistance of Mr. Frank J. Stoddard in studying this aspect.

present. The Mach number profiles were then reduced to velocity profiles assuming that there was no heat transfer from the wall, that is, a constant total enthalpy through the boundary layer. Rigorously this assumption is not true because the inviscid total enthalpy downstream of the centered expansion wave is about 10% less than the wall enthalpy. The consequence of the constant total enthalpy assumption was checked by assuming a Mach number distribution and then computing the velocity profiles first for a constant total enthalpy boundary layer and then for a boundary layer in which the velocity and total enthalpy profiles were similar. For the test conditions used here, the difference between the two velocity profiles was greatest near the wall and was less than 5%. It was concluded from this that it was sufficiently accurate to assume the total enthalpy was constant through the viscous layer.

All reference conditions used in presenting the data, such as Reynolds number and dynamic pressure, are computed for conditions at the leading edge of the model, M = 1.0. The wall temperature ratio was T_w/T_o=1.11 for all experiments.

Results

Shock-Free Conditions

The first experiments were made to check on the pressure distribution on the flat plate ahead of the observation section and to determine the characteristics of the undisturbed boundary layer. The pressure distribution data, shown in Fig. 10, have been divided by the measured total pressure, p_o, and are plotted as a function of the nondimensional axial distance from the leading edge. The effective chord length, c, was taken to be 181 inches so that the nondimensional position of the shock wave, $x/c \approx 0.52$, is the same as that observed in other experiments with the airfoil. The line identified as theory is a fairing of the flight test pressure distribution and is the theoretical curve used to design the porosity distribution. The data shown are for the high Reynolds number condition. Other experiments made at a Reynolds number, based on shock position, of 9 million are in good agreement with these data. It can be seen that the experimental data points are in good agreement with the theoretical curve, and in general they fall slightly below the theoretical curve. The one exception is the data obtained at the location furthest upstream; these points fall about 20% below the curve. The source of this behavior is not certain, but it is clear that it is not due to local flow separation. Skin friction measurements made at the same position showed the flow was attached, and the skin friction was in good agreement with theory. This anomoly in the pressure distribution near the leading edge has been discounted since it is far removed from the observation section and since the skin friction data indicate an attached flow and a normal skin friction.

Pitot and static pressure surveys were made in the undisturbed boundary layer nominally at the chordwise location of the shock holder. The pressure profiles and the velocity profiles inferred from these data are shown in Fig. 11 and 12. Each of the pressure profiles was measured in three separate experiments with different rake assemblies. The pressure profiles show that the boundary layer is repeatable between experiments and it is possible to obtain meaningful data using this survey technique.

The velocity profiles, Fig. 12, provide a useful check on the undisturbed turbulent boundary layer. In order to make this check, the data were first fitted to a power-law profile and determined the exponent to be n = 7.80 and 8.46 at Reynolds numbers, based on shock location, 9 and 36 million respectively. This increase in exponent with Reynolds number is consistent with Little's data[10] obtained on the wall of a wind tunnel. A direct comparison is not possible because it is difficult to determine a length Reynolds number for Little's experiment.

A further check on the undisturbed profiles was made by graphically integrating the velocity profiles to determine the momentum thicknesses, and then comparing these with theoretical predictions. The theories used were Goldstein's imcompressible result[11] as given by Stratford[12], and an empirical generalization of the Spaulding and Chi theory[13]. The empirical generalization was made by noting that Spaulding and Chi's correlation is accurately represented by the relation

$$F_c C_f = \frac{0.0384}{(F_{R_x} Re_x)^{1/6}} \tag{3}$$

with errors of less than 10% over the Reynolds number range used by Spaulding and Chi. This relation was used in the two-dimensional momentum equation, assuming no pressure gradient, i.e., $C_f = 2 d\theta/dx$, and was integrated to infer the following relation for the momentum thickness.

$$\theta = \frac{0.0230x}{F_c (F_{R_x} Re_x)^{1/6}} \tag{4}$$

Table I
Boundary Layer Thicknesses

Reynolds No.	θ (in.) Exp.	θ (in.) Incomp.	θ (in.) Comp.	δ (in.)
9×10^6	.1103	.1412	.1073	1.364
36×10^6	.1021	.1070	.1001	1.334

A comparison is made in Table I between the experimental and theoretical momentum thickness. It can be seen that Goldstein's incompressible theory predicts values about 28% and 5% greater than the experimental values for the two Reynolds numbers. In contrast, the Spaulding and Chi compressible theory predicts values 3% and 2% less than the experimental values. The consistent agreement between compressible theory and experiment is due to the fact that this theory accounts for important Mach number effects on the local skin friction.

Included in Table I is a tabulation of the undisturbed boundary layer thickness. These were computed from the experimental momentum thickness, using the power law exponents given in Fig. 11, and using an expression for θ/δ which accounted for density variations through the boundary layer. These computed boundary layer thicknesses agree to within a few percent with those determined directly from the velocity profiles.

Shock Wave-Boundary Layer Interaction

The experiments with a shock wave interacting with the turbulent boundary layer were made by choking the downstream exit of the apparatus and positioning a normal shock wave at a fixed position in the channel, Fig. 2. The experiments included high speed schlieren motion pictures of the flowfield, chordwise surveys of the surface pressure and skin friction, and pitot and static pressure surveys across the viscous layer. These measurements were used first to obtain an indirect check on the two-dimensionality of the interaction experiment. This check parallels the procedure used by other authors[14,15] and is based on the chordwise integration of the two-dimensional compressible momentum equation,

$$\frac{p_e M_e^2}{(p_e M_e^2)_i}\ \frac{\theta}{\theta_i} - 1 = \int_{x_i}^{x} \frac{C_f}{2}\frac{dx}{\theta_i} + \int_{x_i}^{x} \frac{\delta^*}{\theta_i}\frac{1}{\gamma M_{e_i}^2}\, d\left(\frac{p_e}{p_{e_i}}\right) \quad (5)$$

where the subscript, i, denotes initial undisturbed conditions. The left hand side of Eq. 5 represents the momentum in the viscous layer and the right hand side represents the forces impressed on the layer. The two sides of Eq. 5 were evaluated from the data obtained at a Reynolds number of 9 million, using the measured skin friction coefficient and the measured surface pressure. The two sides of the equation are compared with each other in Fig. 13. It can be seen that the agreement between the two sides of Eq. 5 is reasonably good throughout most of the flowfield, and some of the observed discrepancies can be attributed to using the surface pressure in the evaluation. Based on previous applications of this momentum balance technique[14,15], the two-dimensionality of the present experiment can be regarded as reasonably good.

Schlieren Observations. As noted earlier, high speed (7000 frames/second) schlieren motion pictures of the flowfield were taken during each experiment, and typical photographs for the two Reynolds numbers are shown in Fig. 14 and 15. The flow is from right to left and the markers at the top of the field are 3-3/4 inches apart and indicate the leading and trailing edges of the wedge-shaped area change defining the shock holder, Fig. 2. The dark spots in the field, which change with time, stem from stresses in the glass windows. The time interval between the first and second photograph in Fig. 14 is about 0.7 milliseconds, and about 1.1 milliseconds elapse between the second and third. The wave upstream of the shock holder is believed to be the leading edge of the lambda wave on the tunnel side wall.

There are two items to note in Fig. 14. First it should be noted that the interaction is steady only in a mean sense, as evidenced by the changes observed in the structure and intersection of the bifurcated lambda wave with the surface. The second photograph shows that the leading edge of the lambda wave is too diffuse to register in the schlieren system. The height of the bifurcation varies somewhat with time, and nominally is about three undisturbed boundary layer thicknesses above the plate. These observations are consistent with the usual concept of a turbulent boundary layer having a thickness which varies with time as turbulent bursts are swept downstream.

The comparable schlieren photographs obtained at the higher Reynolds number are shown in Fig. 15. The preceding comments on steadiness are seen to apply here too. The important feature to note between Fig. 14 and 15 is the decrease in the height of the bifurcation with increasing Reynolds number: it decreases by a factor of two and nominally is about 2-1/2 undisturbed boundary layer thicknesses in height at the higher Reynolds number. This behavior suggests that the upstream influence of the shock wave will be diminished at the higher Reynolds number.

Surface Pressure and Skin Friction. The chordwise distributions of surface pressure and skin friction coefficient are shown in Fig. 16 and 17. The distance coordinate in each case is measured from the position of the shock holder, and this corresponds nominally to the location of the normal portion of the shock wave. This is used, in preference, to the leading edge of the lambda shock, because of the unsteadiness observed in the shock structure near the surface. The data obtained at $Re_s = 9 \times 10^6$ show that interaction is quite diffuse and extends about 4-1/2 δ_u upstream of the normal shock wave. The point where the first disturbance is observed in the surface pressure is in good agreement with the most forward excursion of the lambda wave observed in the schlieren photographs, Fig. 14. The pressure data obtained at the most forward positions agree well with data obtained in undisturbed flow, thereby indicate the position of the first disturbance. It can be seen in Fig. 16 that the surface pressure increases gradually but does not reach the normal shock limit in the region surveyed.

The skin friction data, obtained at the most forward survey station, Fig. 16, agree well with Spaulding and Chi theory[13] and thereby indicate that the flow was undisturbed at that location. The upstream effect on the skin friction is to produce a rapid decrease and then an increase towards the undisturbed value at about 2 δ_u upstream of the shock wave. This is followed by a rapid decrease in skin friction over a chordwise distance of about 1 δ_u, and separation begins about 1 δ_u ahead of the shock wave. The separated region at this Reynolds number is a total of 12 inches long, or about 8-3/4 δ_u. The points corresponding to separation and reattachment are indicated on the pressure distribution in Fig. 16, and it is seen that there are distinct kinks at these points. This correspondence between pressure kinks and the details of the separated region have been noted earlier by Pearcey[16].

It should be noted that the skin friction data in Fig. 16 are steady only in a mean sense, and that there is a fluctuating component that is equal to about ±10 to 15% of the undisturbed skin friction coefficient. This implies that the separation and reattachment points are not steady, but rather they fluctuate about a mean point on the surface. The small negative values of skin friction near separation suggests that the chordwise excursion of the separation point could be quite large. These observations are consistent with the unsteadiness noted in the schlieren photographs.

The skin friction and surface pressure data obtained at $Re_s = 36 \times 10^6$ are shown in Fig. 17. These data show some features similar to those in Fig. 16 and some that are very different. The pressure data indicate a weak disturbance about 5 δ_u ahead of the shock wave, similar to the behavior in Fig. 16, but the pressure rises to a plateau about 10% greater than the undisturbed value and remains there until about 1 δ_u ahead of the shock where a rapid increase in pressure begins. The overall pressure rise exceeds that in Fig. 16 but it does not reach the normal shock wave limit. It should also be noted that the leading edge of the lambda wave in Fig. 15 does not coincide with the chordwise position of the first pressure disturbances as at the low Reynolds number, but intersects the surface about 3 δ_u ahead of the shock wave where the pressure shows a plateau.

The skin friction data, Fig. 17, obtained at the most forward location are seen to be in good agreement with Spaulding and Chi theory[13], suggesting that the flow there is undisturbed. There is a gradual decrease and then a slight increase in skin friction up to about 1 δ_u ahead of the shock wave, and this is followed by a gradual decrease in skin friction over a chordwise distance of about 2 δ_u to separation. However in this case, the separated region is confined to a region only about 2 δ_u in chordwise extent. It should also be noted that separation in this instance is characterized by a negative mean skin friction coefficient which is quite small. In view of the previous observations on the magnitude of the fluctuating component of the skin friction, the implication is that the entire separated region is unsteady and is separated only in a mean sense. The points corresponding to flow separation and reattachment are indicated on the pressure distribution, and it can be seen that these events again are accompanied by kinks in the pressure distribution.

The data in Fig. 16 and 17 have been used to test the theories of Gadd[17] and of Stratford[12]. Gadd's theory is approximate in that it is based on a number of simplifying assumptions both for the inviscid flow and for the viscous layer. In addition, it is restricted to inviscid supersonic Mach numbers, $M \leq 1.3$. One result given by Gadd is for the skin friction distribution in the upstream portions of the interaction.

$$\frac{C_f}{C_{f_i}} = \left\{ \frac{(n+2)\,\frac{M_1}{M_e}\left(\frac{T_1}{T_e}\right)^{\frac{\gamma+1}{2(\gamma-1)}}}{(n+3)\left(\frac{M_e}{M_1}\right)^2 - 1} \right\} \left\{ 1 + \frac{2.5x}{M_e}\frac{dM_e}{dx}\left[\frac{1 - \frac{\gamma-1}{2}M_e^2\frac{\theta}{\delta}}{(n+3)\left(\frac{M_e}{M_1}\right)^2 - 3} - \frac{1}{(n+3)\left(\frac{M_e}{M_1}\right)^2 - 1} \right] \right\} \tag{6}$$

This result was applied to the present experimental data using the pressure data shown in Figure 16 and 17 to determine the local Mach number and local gradient of Mach number. This is in keeping with the spirit of Gadd's analysis since he assumes the static pressure variations through the viscous layer are small. The exponents for the undisturbed boundary layer were obtained from the data shown in Figure 12, and hence they include the effect of Reynolds number on this parameter. The comparison between the theoretical and experimental skin friction distributions is shown in Fig. 18, and it can be seen that at the lowest Reynolds number, Gadd's theory predicts the initial skin friction behavior reasonably well in that it predicts the location and magnitude of the decrease in skin friction. However, the theory does not predict the subsequent increase in skin friction prior to separation, and in fact, it does not indicate separation at any point in the flowfield. Of course, the theory does not apply throughout the entire flowfield, and the downstream comparison is included here only for completeness.

The comparison between theory and experiment at the higher Reynolds number, Figure 18, shows a different trend. Theory predicts an initial increase in skin friction but the experimental data show an initial decrease. The theory shows a rapid approach to separation and when applied to the subsonic portion of the flow field predicts reattachment at about the correct chordwise position. The predicted size of the separated region is about twice the length observed experimentally.

The separation criterion given by Stratford[12] was also tested with the present data. Stratford's criterion is based upon a flat plate model in which the turbulent boundary layer develops under a constant pressure. The boundary layer at the end of this constant pressure development is treated as two layers in which viscosity dominates in the layer near the wall and the dynamic terms dominate in the outer layer. It should be noted that the present experiment is a good test for Stratford's model in that the boundary layer develops on the flat plate under nearly constant pressure conditions.

Stratford derives his criterion for boundary layers described by a 1/7 power law. This is a reasonable choice for moderate Reynolds numbers, but can be substantially in error at high Reynolds numbers. Consequently, the criterion was re-derived here for an arbitrary power law. This generalized criterion is

$$(C_p)^{\frac{n-2}{4}}\sqrt{x\frac{dC_p}{dx}} = \left(\frac{n-2}{n+1}\right)^{\frac{n-2}{4}}\left(\frac{3}{n+1}\right)^{1/4}\frac{2.161\beta\,(Re_x)^{1/10}}{\sqrt{(n+1)(n+2)}} \tag{7}$$

where $\beta = 0.66$ is an empirical constant.

The criterion in Equation 7 was evaluated using the pressure data from Figure 16 and 17, and using the power law exponents given in Figure 12. The pressure coefficients and the separation criterion are given in Figure 19. Separation is predicted to occur if the parameter, $(C_p)^{(n-2)/4}\sqrt{x\,dC_p/dx}$ exceeds the value given by the right side of Eq. 7, nominally 0.32 and 0.33 for the two cases shown in Fig. 19. It can be seen that this parameter reached somewhat higher values in the present experiments, suggesting that the empirical constant should have a higher value. It should be noted, however, that

the difference between the theoretical and experimental separation points nominally is 1 δ_u.

Velocity Profiles. Pitot and static pressure surveys were made in the interaction zone and these were used to infer the velocity profiles. A reversed rake was used in an attempt to determine the profiles in the regions with reversed flow, but it was found that the difference between pitot and static pressure could not be resolved. This is consistent with Seddon's results[18] which show that the maximum Mach number in the reverse-flow region is about 0.09, and consequently the maximum difference between the pitot and static pressure is about 0.5%.

Typical pressure profiles obtained with forward facing rakes at the leading edge of the separated region are shown in Fig. 20. These illustrate one difficulty encountered when interpreting measurements obtained in a separated region, namely that the pitot pressure measured with a forward-facing rake is consistently 2% to 5% greater than the static pressure. This difference is believed to stem from the interpretation given to the mean measurement of pitot pressure in a turbulent flow. This is illustrated by writing down the expression for the instantaneous value of the pitot pressure in terms of the fluctuating quantities, and then time-averaging that relation. This calculation shows that when the mean velocity goes to zero, the pitot pressure becomes

$$\overline{p_o} = \bar{p} + \frac{1}{2}\left(\bar{\rho}\,\overline{u'^2} + \overline{\rho' u'^2}\right) \qquad (8)$$

where the prime denotes the fluctuating components and the bar denotes time-averaged quantities. For the present measurements $\bar{p}$ is the base pressure for the pitot rake in reversed flow. This was estimated using the criterion given by Hoerner[19], and that calculation showed that the base pressure should differ from the local static pressure by about 0.01%. Consequently, $\bar{p}$ can be taken as the local static pressure. The time-averaged values of the fluctuating terms should be dominated by the first term, $\bar{\rho}\,\overline{u'^2}$, because the second term is of higher order. Schlicting[20] presents low speed data obtained by Reichardt[21] and by Klebanoff[22] in flat plate boundary layers showing that $\sqrt{\overline{u'^2}}$ reaches a maximum value near the surface that is about 10% to 15% of the free-stream velocity. This is comparable with the differences observed in Fig. 20. The higher values in the present experiment, 15% to 20% of the free stream velocity, could stem from higher turbulence levels associated with the shock wave interaction. The conclusion is that the differences between pitot and static pressure observed here stem from the velocity fluctuations in the turbulent flow, and the magnitude of these differences is consistent with published data.

The effects of the fluctuating velocity components were neglected in reducing the present data to local Mach number and local velocity. The pitot pressure data were faired, as indicated in Fig. 20, to estimate the stream surface where the mean velocity was zero.

Velocity profiles obtained at a Reynolds number Re_s, of 9 million are presented in Fig. 21a to 21d. The local velocity has been divided by the velocity at the apparent edge of the viscous layer, and the vertical coordinate has been divided by the thickness of the undisturbed boundary layer, δ_u. The distance, x_s, is measured from the normal shock wave and is positive downstream of the shock wave. A sketch of the shock configuration, taken from the last frame in Fig. 14, is shown on these figures along with the relative positions of the survey stations.

The data obtained in the interaction zone ahead of separation are compared with the undisturbed profile in Fig. 21a. It can be seen that the profiles are progressively retarded as the flow approaches the shock wave, indicating an approach to separation. These general characteristics are in qualitative agreement with the skin friction data, Fig. 16, in that they indicate a shear stress smaller than the undisturbed value. It should be noted that the undisturbed profile was obtained in experiments without an interacting shock wave. Consequently, the data in Fig. 21a do not define the upstream limit of disturbances from the shock wave. One further item to note in Fig. 21a is that the profile obtained at station 2 does not indicate a uniform velocity for $y/\delta_u < 2$. This behavior is believed to reflect the fact that the survey was made within the bifurcated shock wave, and the small velocity defect is that caused by the oblique portion of the shock wave.

The profiles obtained in the region with flow separation are shown in Fig. 21b to 21d. The data obtained at station 3 indicate the flow is separated and data obtained one inch further forward, not shown here, indicate an unseparated flow. This finding is in good agreement with the skin friction data. The profile at station 3 also exhibits a gradual approach to the undisturbed velocity. Again this is ascribed to the fact that the profile was obtained just ahead of the normal shock wave and in the thickest portion of the bifuracted shock wave. The flow at this survey station is sonic at $y/\delta_u \approx 1.0$, and the ambient undisturbed Mach number is observed at $y/\delta_u > 3.5$.

The profile at station 4 exhibits an overshoot in that the local velocity at $y/\delta_u \approx 1.5$ exceeds the velocity at the edge of the viscous layer. This somewhat analogous to the supersonic tongue observed by Seddon[18]; however, the flow at this survey station and the other downstream stations was entirely subsonic. This is markedly different from Seddon's results, in that he finds a supersonic tongue extending about 8 δ_u downstream from the normal shock wave. This probably stems from the differences in ambient conditions; M = 1.47 and $Re_s = 3 \times 10^6$ for Seddon's experiments.

The profiles obtained near the axial center of the separation bubble, Fig. 21c, show that the thickness of the bubble is relatively constant and show the profile variations with axial position are relatively small. Fig. 21d illustrates the profiles as the flow approaches reattachment, and they show that the bubble becomes thinner and that the flow is reattached at station 11, $x/\delta_u = 7.5$. This finding is in good agreement with the skin friction data, Fig. 16. However, it will be noted in Fig. 21d that the inferred velocity near the surface at station 11 is nearly constant. This behavior apparently stems from difficulties in interpreting the pitot-static near the surface. The pitot data

indicate attached flow in that they show a smooth and continuous profile. However, there are rapid variations in the static pressure near the surface, and the net result is that shown in Fig. 21d. It is believed that the apparent contradiction between the pitot profile and the inferred velocity profile is produced by the effect of the fluctuating terms in Eq. 8 on the pitot pressure. If this contention is correct, it would imply that the fluctuating velocity component at reattachment is $\sqrt{\overline{u'^2}} \approx 1/3\, u_e$ This is two to three times greater than the published data for undisturbed turbulent boundary layers[21,22].

Typical velocity profiles obtained in the interaction zone at a Reynolds number, Re_s, of 36 million are shown in Fig. 22. The sketch of the shock wave configuration, shown there, is taken from the last frame in Fig. 15. The velocity data obtained at the leading edge of the bifurcated shock wave, station 1, indicate that the profile is generally retarded and that the surface shear stress is less than the undisturbed value. This is in qualitative agreement with the skin friction data in Fig. 17. The data obtained downstream of the normal shock wave, Fig. 22b, indicate that the flow is separated at $x_s/\delta_u = .94$, confirming the skin friction data in Fig. 17. Profile data obtained one inch ahead of station 2, not shown here, indicate an attached flow.

There are several items to be noted in Fig. 22b. First, the indicated edge of the separated region is greatest at Sta. 2, near the leading edge of the separated region, and the thickness of the separated region decreases in the downstream direction. Second, there is a marked overshoot in the profiles in that the local velocity at $y/\delta_u \approx 1.25$ exceeds the velocity at the apparent edge of the viscous layer by as much as 22%. This behavior is similar to that observed at the lower Reynolds number, Fig. 21b, except the magnitude of the overshoot is at least three times larger and it persists to all downstream stations reported here. Again, this overshoot is analogous to Seddon's supersonic tongue[18] except all of the profiles in Fig. 22b were subsonic. Finally, it should be noted that the surveys shown in Fig. 22b do not extend far enough above the surface to identify clearly the apparent edge of the viscous layer. This implies that the velocity overshoot could be larger than indicated here.

The velocity profiles shown in Fig. 22c indicate that the flow is reattached at $x_s/\delta_u = 3.19$, again confirming the skin friction data, Fig. 17. It can be seen that the velocity overshoot persists to these downstream stations, but is gradually diminished to about 3% at $x_s/\delta_u = 4.69$. The data in Fig. 22c also indicate a progressive retardation in the profiles in the downstream direction. Experiments are in progress to further investigate this downstream behavior.

Concluding Remarks

The purpose of this experimental research, which is still in progress, has been to investigate the influence of Reynolds number of the shock wave - turbulent boundary layer interaction that occurs on an airfoil at transonic speeds. The pertinent features of this transonic airfoil problem have been duplicated in a two-dimensional, large-scale simulation experiment by using a flat plate in a suitably modified supersonic nozzle to obtain the desired axial pressure distribution. The downstream exit of the apparatus is choked to position a normal shock wave at the desired axial position. Experiments made without an interacting shock wave showed that the desired pressure distribution was obtained, and that the characteristics of the undisturbed boundary layer were in good agreement with compressible boundary layer theory.

The experiments with an interacting shock wave were made with a local Mach number ahead of the shock nominally 1.4, and at Reynolds numbers of 9 million and 36 million. The surface pressure data and skin friction data shown large changes with Reynolds number. At the lower Reynolds number, the compression due to the shock wave is very gradual and begins about 5-1/2 boundary layer thicknesses upstream of the shock wave. The first disturbance is indicated at about the same location upstream at the higher Reynolds number, but the strong compression zone begins about one boundary layer thickness upstream of the shock wave. The skin friction data shows that the chordwise extent of the separated region decreases markedly with Reynolds number, from about nine to about two boundary layer thicknesses.

The velocity profiles obtained in the immediate vicinity of the shockwave qualitatively confirm the surface measurements. They show that for these conditions, there is velocity overshoot immediately downstream of the shockwave, analogous to Seddon's observations of a supersonic tongue, but the entire flowfield surveyed here was found to be subsonic. This velocity overshoot increased both in magnitude and in downstream extent with increasing Reynolds number.

High-speed schlieren motion pictures indicate that the interaction is steady only in a mean sense in that the structure of the bifurcated shockwave changes with time. These also show that the height of the bifurcation decrease from about 4-1/4 to about 2-1/2 undisturbed boundary layer thicknesses as the Reynolds number is increased from 9 million to 36 million.

References

1. Loving, D.L., "Wind-Tunnel-Flight Correlation of Shock-Induced Separated Flow" NASA TND-3580, September 1966.

2. Ludwieg, H., "Tube Wind Tunnel, A Special Type of Blowdown Wind Tunnel" AGARD Report 143, July 1957

3. Falk, T.J., "A Tube Wind Tunnel for High Reynolds Number Supersonic Testing" ARL Report 68-0031 (Also Calspan Report AD-2297-A-1) February 1968

4. Sheeran, W.J. and Hendershot, K.C. "A New Concept of a Variable-Mach-Number Perforated Wall Nozzle for Providing a Supersonic External Stream in Rocket-Propulsion Testing" AIAA Paper 68-238, March 1968

5. Russo, A.L. and Hertzberg, A., "Modifications to the Basic Shock Tube to Improve Its Performance" Calspan Report AD 1052-A-7 Aug. 1958

6. Fetz, B.H., "Analysis of the Optimum Performance of Buffered Shock Tubes" ARL Report 64-41 March 1964

7. Bogdan, L., "Instrumentation Techniques for Short-Duration Test Facilities" Calspan Report No. WTH-030, March 1967

8. MacArthur, R.C., "Contoured Skin Friction Transducers" Calspan Report No. AN-2403-Y-1 August 1967

9. Davies, W.R. and Bernstein, L., "Heat Transfer and Transition to Turbulence in the Shock-Induced Boundary Layer on a Semi-Infinite Flat Plate" J. Fluid Mech., Vol. 36, Pt. 1, 1969 pp. 87-112

10. Little, B.N., "Effects of Initial Turbulent Boundary Layer on Shock-Induced Separation in Transonic Flow" Von Karman Institute for Fluid Dynamics, Tech. Note 39, Oct. 1967

11. Goldstein, S. Modern Developments in Fluid Dynamics, Oxford University Press, 1938

12. Stratford, B.S., "The Prediction of Separation of the Turbulent Boundary Layer" J.F.M. Vol. 5, Pt. 1, Jan. 1959, pp. 1-16

13. Spaulding, D.B. and Chi, S.W., "The Drag of a Compressible Turbulent Boundary Layer on a Smooth Flat Plate With and Without Heat Transfer" J.F.M., Vol. 18, Pt. 1, Jan. 1964, pp. 117-143

14. Coles, D.E. and Hurst, E.A., "Computation of Turbulent Boundary Layers - 1968", AFOSR-IFP-Stanford Conference, Vol. 2., Dept of M.E., Stanford Univ., 1969

15. Alber, I.E., Bacon, J.W., Masson, B.S., and Collins, D.J., "An Experimental Investigation of Turbulent Transonic Viscous-Inviscid Interactions" AIAA Jour., Vol. 11, No. 5, May 1973, pp. 620-627

16. Pearcey, H.H., "Some Effects of Shock-Induced Separation of Turbulent Boundary Layers in Transonic Flow Past Airfoils" In Boundary Layer Effects in Aerodynamics, Symposium held at National Physical Laboratory, April 1955

17. Gadd, G.E., "Interactions Between Normal Shock Wave and Turbulent Boundary Layers" ARC 22, 559, Feb. 1961

18. Seddon, J., "The Flow Produced by Interaction of a Turbulent Boundary Layer with a Normal Shock Wave of Strength Sufficient to Cause Separation." ARC R & M No. 3502 March 1960

19. Hoener, S.F., Aerodynamic Drag, The Otterbein Press, Dayton, 1951

20. Schlicting, H., Boundary Layer Theory, Fourth Edition, McGraw Hill, Inc., New York, 1960, pp. 466-467

21. H. Reichardt. Messungen turbulenter Schwankungen Naturwissenschaften 404 (1938); see also ZAMM 13, 177 (1933) and ZAMM 18, 358 (1938).

22. P.S. Klebanoff, Characteristics of turbulence in a boundary layer with zero pressure gradient NACA Rep. No. 1247 (1955)

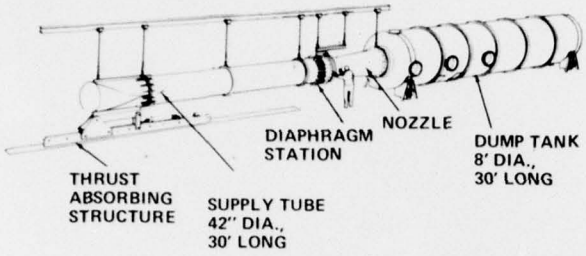

Figure 1 CALSPAN LUDWIEG TUBE

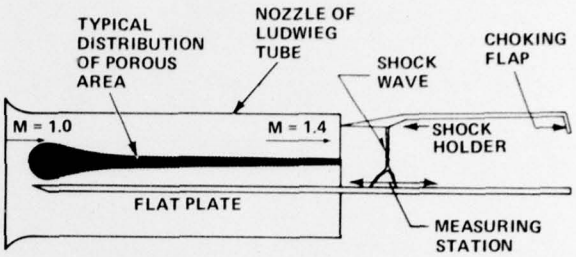

Figure 2 SCHEMATIC OF THE SHOCK WAVE – BOUNDARY LAYER INTERACTION EXPERIMENT IN THE CALSPAN LUDWIEG TUBE

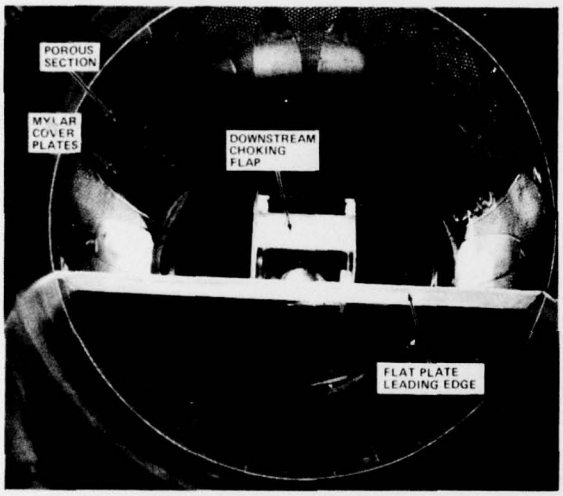

Figure 3 VIEW FROM NOZZLE ENTRANCE OF MODEL ASSEMBLY

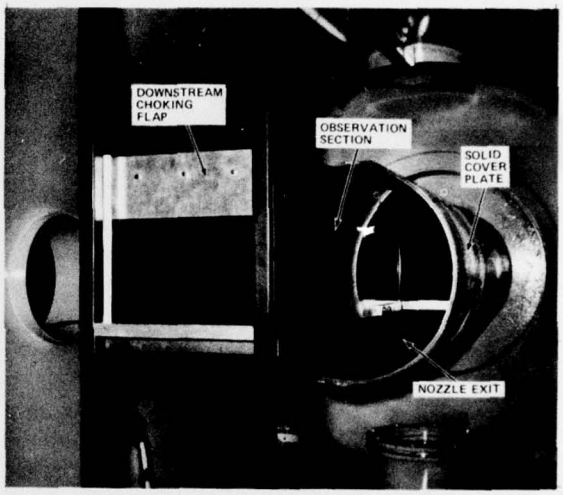

Figure 4 NOZZLE EXIT WITH INSTALLED MODEL ASSEMBLY

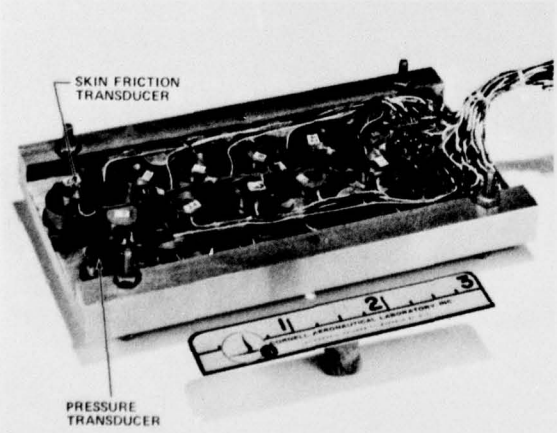

Figure 5 INSTRUMENTATION SURFACE OF THE SKIN FRICTION-SURFACE PRESSURE SURVEY PLATE

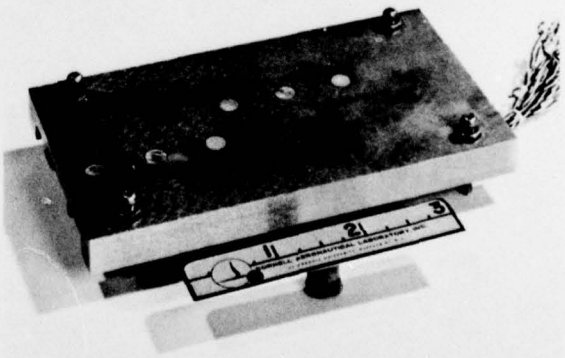

Figure 6 EXPOSED SURFACE OF THE SKIN FRICTION-SURFACE PRESSURE SURVEY PLATE

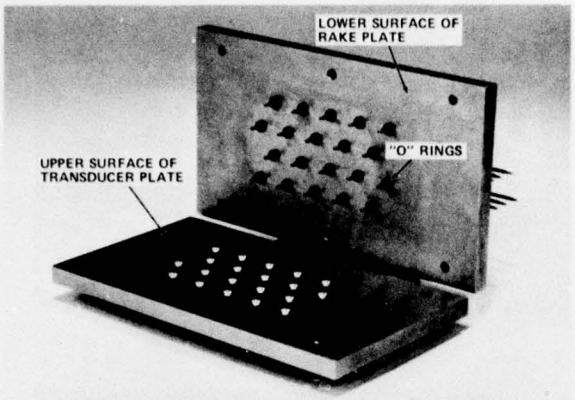

Figure 7 TRANSDUCER PLATE AND RAKE PLATE ASSEMBLY

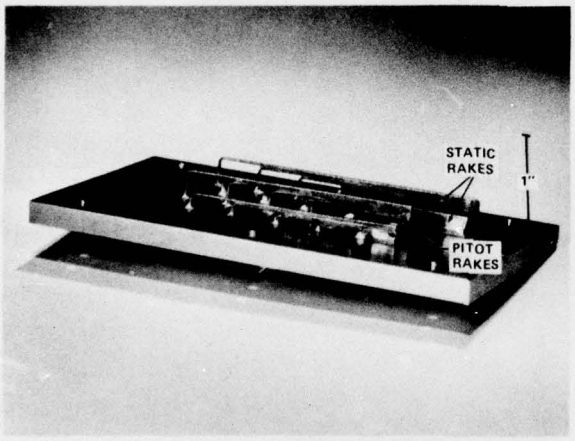

Figure 8 PITOT–STATIC SURVEY RAKES

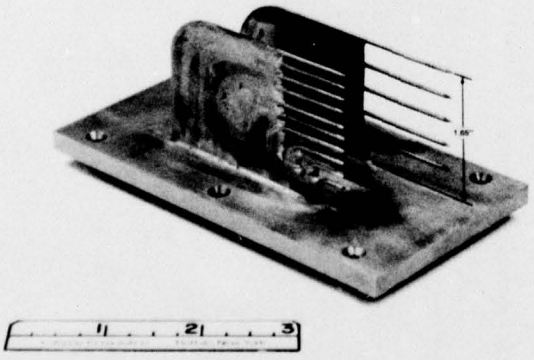

Figure 9 PITOT–STATIC SURVEY RAKES

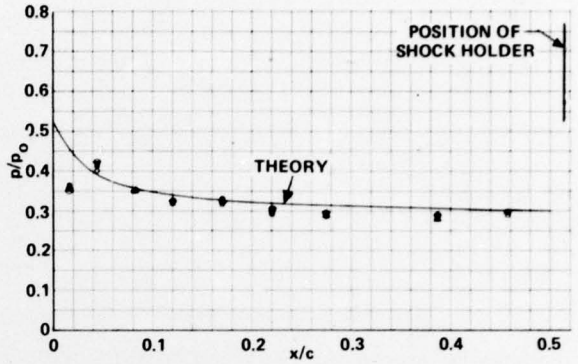

Figure 10 PRESSURE DISTRIBUTION ON THE FLAT PLATE, Re = 4.6 x 10^6/FT

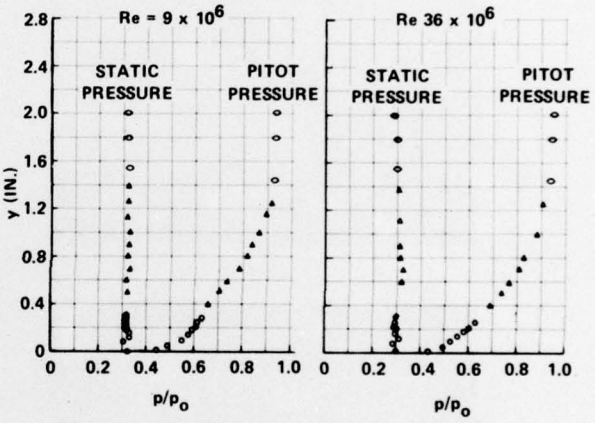

Figure 11 UNDISTURBED PRESSURE PROFILES

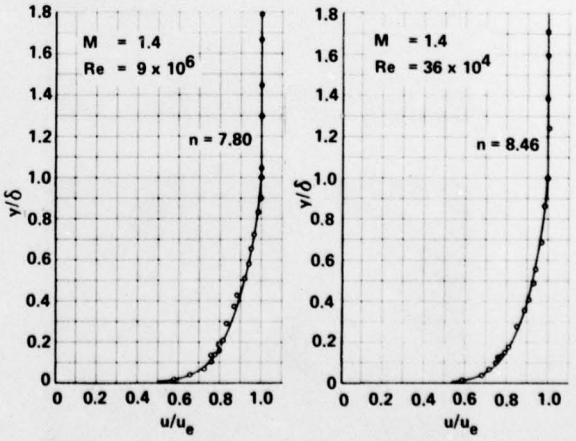

Figure 12 UNDISTURBED BOUNDARY LAYER PROFILES

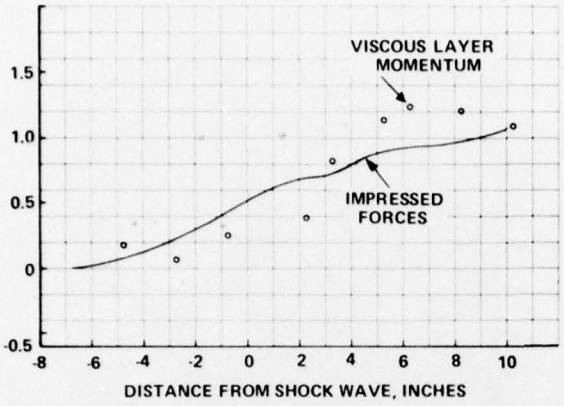

Figure 13 EXPERIMENTAL MOMENTUM BALANCE

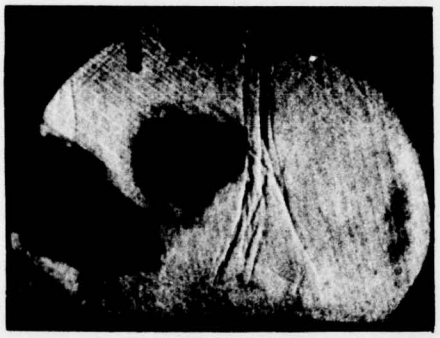

(a)

(b)

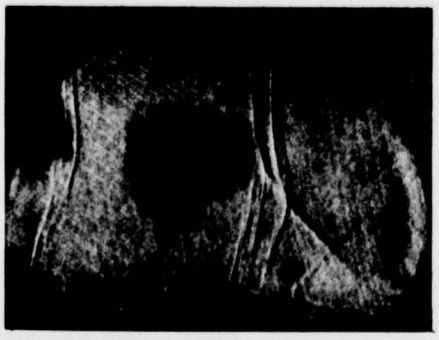

(c)

Figure 14 FLOW FIELD FOR $Re_S = 9 \times 10^6$

(a)

(b)

Figure 15 FLOW FIELD FOR $Re_S = 36 \times 10^6$

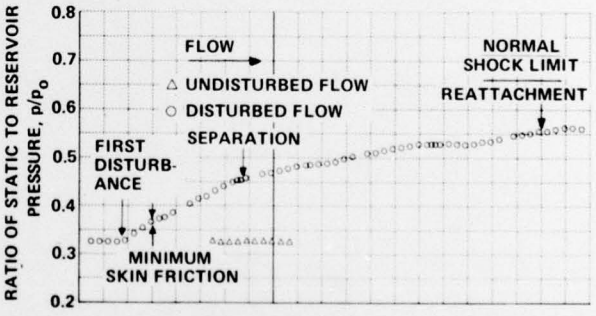

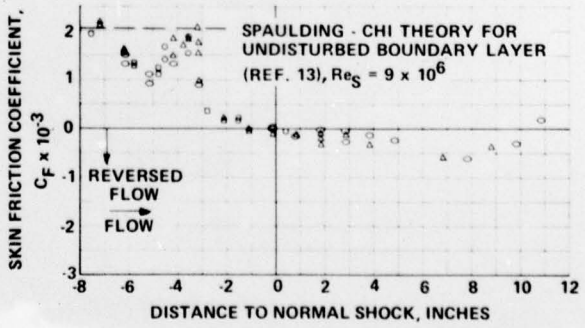

Figure 16 SURFACE PRESSURE AND SKIN FRICTION DISTRIBUTIONS IN THE INTERACTION ZONE

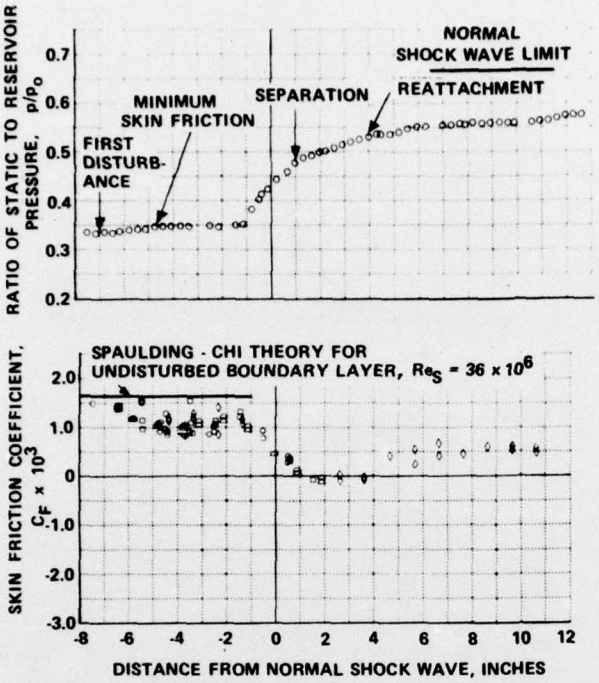

Figure 17 SURFACE PRESSURE AND SKIN FRICTION DISTRIBUTIONS IN THE INTERACTION ZONE

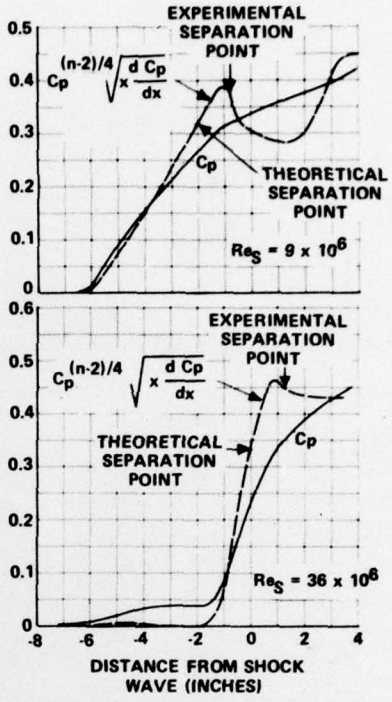

Figure 19 EVALUATION OF STRATFORD'S SEPARATION CRITERION

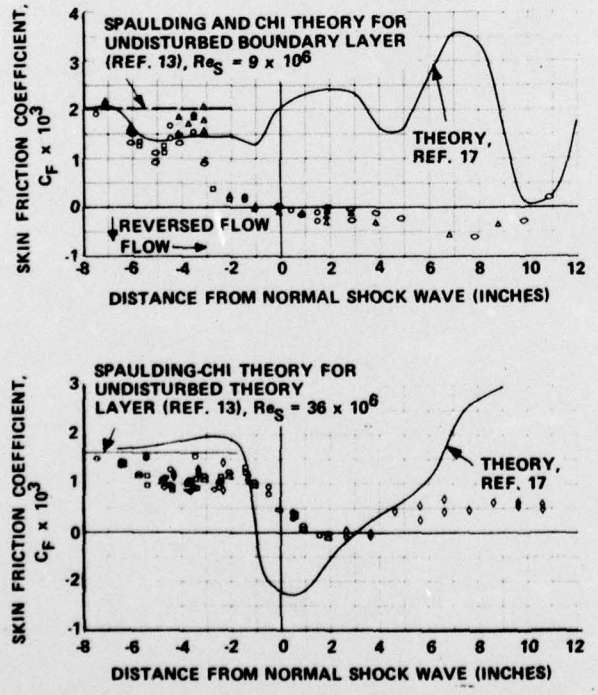

Figure 18 LOCAL MACH NUMBER AND SKIN FRICTION DISTRIBUTION IN THE INTERACTION ZONE

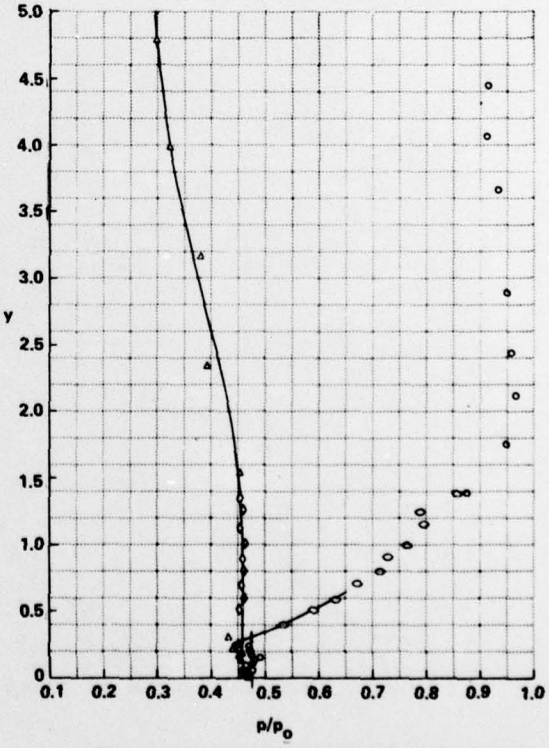

Figure 20 PITOT-STATIC PRESSURE PROFILES IN INTERACTION ZONE, Re$_S$ = 9 x 10^6 X$_S$ = 0.74 INCHES

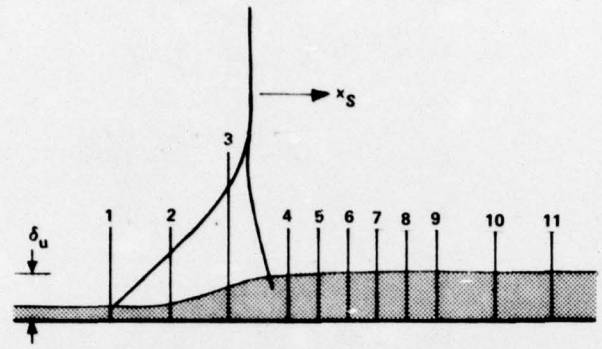

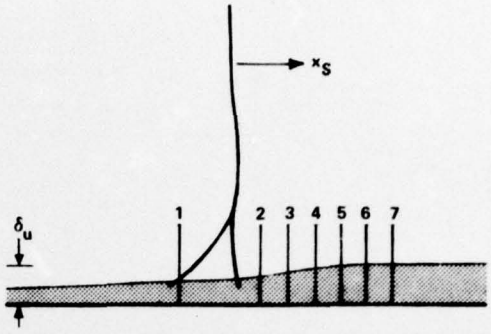

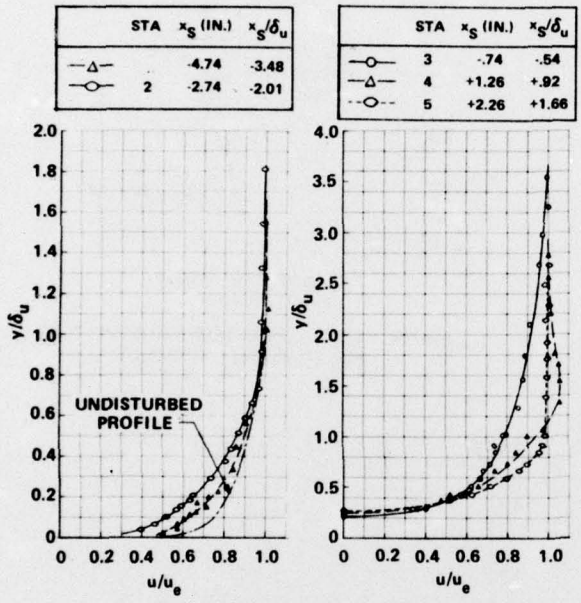

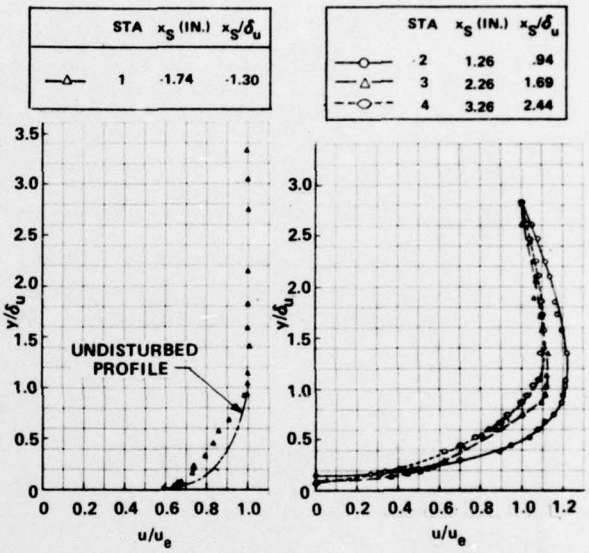

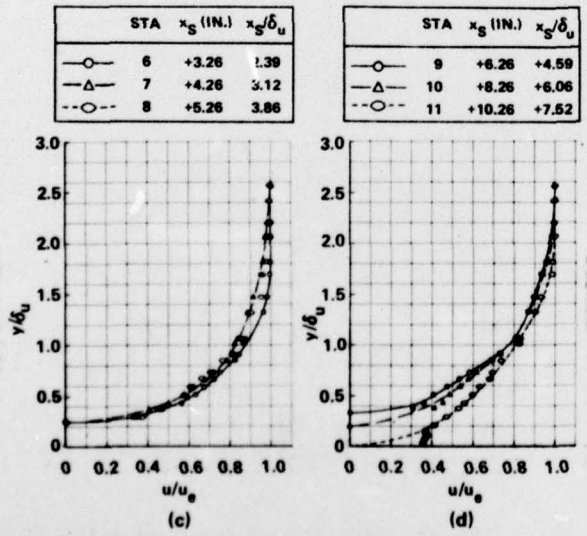

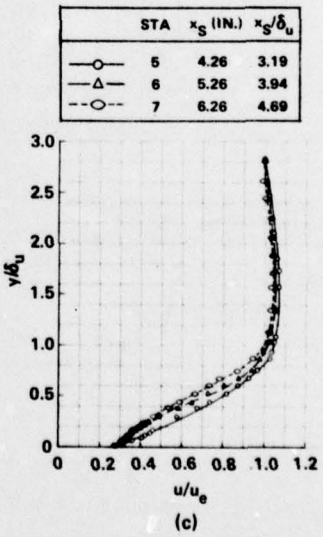

Figure 21 VISCOUS LAYER PROFILES IN THE INTERACTION ZONE $Re_S = 9 \times 10^6$

Figure 22 VISCOUS LAYER PROFILES IN THE INTERACTION ZONE $Re_S = 36 \times 10^6$